Fire Technology manuscript No.
(will be inserted by the editor)

Sensors and Machine Learning Models to Prevent Cooktop Ignition and Ignore Normal Cooking

Amy E. Mensch · Anthony Hamins · Wai Cheong Tam · Z.Q. John Lu · Kathryn Markell · Christina You · Matthew Kupferschmid

Received: 19 March 2020 / Accepted: 26 February 2021

Abstract Cooking equipment is involved in nearly half of home fires in the United States, with cooktop fires the leading cause of deaths and injuries in cooking-related fires. In this study, we evaluate 16 electrochemical, optical, temperature and humidity sensors, placed in the cooktop exhaust duct, for use in predicting and preventing cooktop ignition. The sensors were evaluated in a series of 60 experiments conducted in a mock kitchen. Experiments covered a broad range of conditions, including both unattended cooking and normal cooking scenarios, where 39 experiments led to auto-ignition. The experiments involved a variety of cooking oils and foods and were conducted using either an electric coil cooktop, gas-fueled cooktop, or electric oven. The sensor data collected in the experiments were used in two types of analysis, threshold analysis and neural-network analysis, to estimate the performance of the sensors for predicting ignition and ignoring normal cooking conditions. The combined information from multiple sensors was evaluated in sensor ratios with threshold analysis, and in the neural-network models developed using selected pairs of sensor inputs. Some of the multiple-sensor cases performed as well as or better than the individual sensor thresholds and individual sensor models. Consistently across threshold and machine learning analysis, the best performing sensor was the sensor measuring volatile organic compounds. This sensor was also included in all of the best performing sensor ratios and machine learning models.[1]

Keywords Cooktop ignition · Sensor analysis · Neural networks · ignition prevention

1 Introduction

According to a recent National Fire Protection Association (NFPA) report, 47 % of reported home fires involve cooking equipment, with cooktops accounting for 87 % of cooking-fire deaths and 80 % of the civilian injuries [1]. Electric-coil stovetops manufactured after June 2018 in the U.S. must pass the abnormal cooking test in Underwriters Laboratories (UL) 858 [2]. The test prescribes a maximum temperature

A. Mensch, A. Hamins, W.C. Tam, Z.Q. Lu, K. Markell, C. You, M. Kupferschmid
100 Bureau Drive
Gaithersburg, MD 20899-8664
Tel.: 301-975-6714
E-mail: amy.mensch@nist.gov

[1] Certain commercial equipment, instruments, or materials are identified in this paper in order to specify the procedures adequately. Such identification is not intended to imply recommendation or endorsement by the National Institute of Standards and Technology, nor is it intended to imply that the materials or equipment identified are necessarily the best available for the purpose.

of the dry-pan or a performance test for ignition-prevention using 50 mL of canola oil with the coil element on its highest power setting. This standard does not apply to older cooktops or other types of cooking appliances, such as gas cooktops.

Therefore, we consider the feasibility of using a variety of sensors as the basis for a retrofit device that would provide early warning or feedback control to automatically shut off the cooktop to prevent ignition. The goal of this device would be to prevent fires from unattended cooking, while ignoring normal-cooking activities and nuisance sources. It may be advantageous to install the proposed system near or within a kitchen exhaust duct or on the ceiling in the kitchen.[2] It could also be integrated into existing household systems via the internet.

There have been studies that investigated the performance advantages of multiple sensors over a single sensor for detection of generalized fire conditions and nuisance-alarm resistance. Gottuk et al. [3] compared the effectiveness of various multi-criteria, fire-detection algorithms using signals from carbon monoxide (CO) sensors and smoke detectors to reduce false fire alarms and to increase detection sensitivity. A cutoff value for the signal of the CO sensor multiplied by the signal from an ionization smoke detector was reported to show improved effectiveness over typical smoke detectors.

In another study, Cestari et al. [4] included the signals from ionization, photoelectric and CO detectors with temperature from a thermocouple to develop advanced, fire-detection algorithms that reduced nuisance sensitivity and detected fires at least as fast as conventional ionization and photoelectric detectors. Eight parameters were identified from the four sensors by considering the magnitude and rate of rise of the output from each sensor. Algorithms developed using these parameters showed that the best fire sensitivity and nuisance immunity was observed for the algorithms based on 1) temperature rise and CO, 2) CO and ionization detector, and 3) temperature rise, CO and ionization detector. Another series of studies developed and tested a prototype four-sensor (ionization, photoelectric, CO and carbon dioxide (CO_2)) package for early warning seaboard applications [5]. Although these studies did not focus solely on cooktop fires, typical, nuisance sources from cooktops were considered, including steam as well as cooking aerosols (e.g., the effluent from hot cooking oil and bacon).

A few studies focused on cooktop fires and considered multi-detector sensing of pre-ignition signatures in a kitchen environment. Johnsson [6] conducted a series of experiments investigating the feasibility of distinguishing between normal-cooking activities and pre-ignition conditions using a variety of sensors in a mock kitchen with a closed door. Sensors were placed above the cooktop and on the compartment ceiling. Signals from alcohol, CO, and hydrocarbon sensors showed the potential to predict ignition while discriminating from normal cooking. Nearly all the experiments were conducted with the range hood off and the effects of room configuration and transport likely played a significant role in the interpretation of results. More recently, Johnsson and Zarzecki [7] conducted experiments that suggested that modified photoelectric smoke detectors could be used to warn of pre-ignition conditions while not impacting normal-cooking scenarios.

Jain et al. [8] conducted cooking-oil auto-ignition experiments, considering the effectiveness of various inexpensive sensors to detect pre-ignition conditions, and reported that the rate-of-change of the moving average of CO concentration was a robust indicator of impending ignition. The study, however, did not consider normal cooking or common, nuisance sources.

The objective of this study was to apply data-driven, statistical methods and machine learning methods to design a detection algorithm for cooktop ignition prevention. Data was obtained from experiments of a variety of ignition and normal-cooking scenarios. The experiments were focused on measuring sensor response, with limited consideration of effluent transport to the sensors. Our approach was to develop and evaluate the performance of sensor-based prediction algorithms using threshold analysis and neural-network models.

[2] Further research may be needed to characterize the long-term performance of a sensor system exposed to a range of typical cooking scenarios and kitchen conditions.

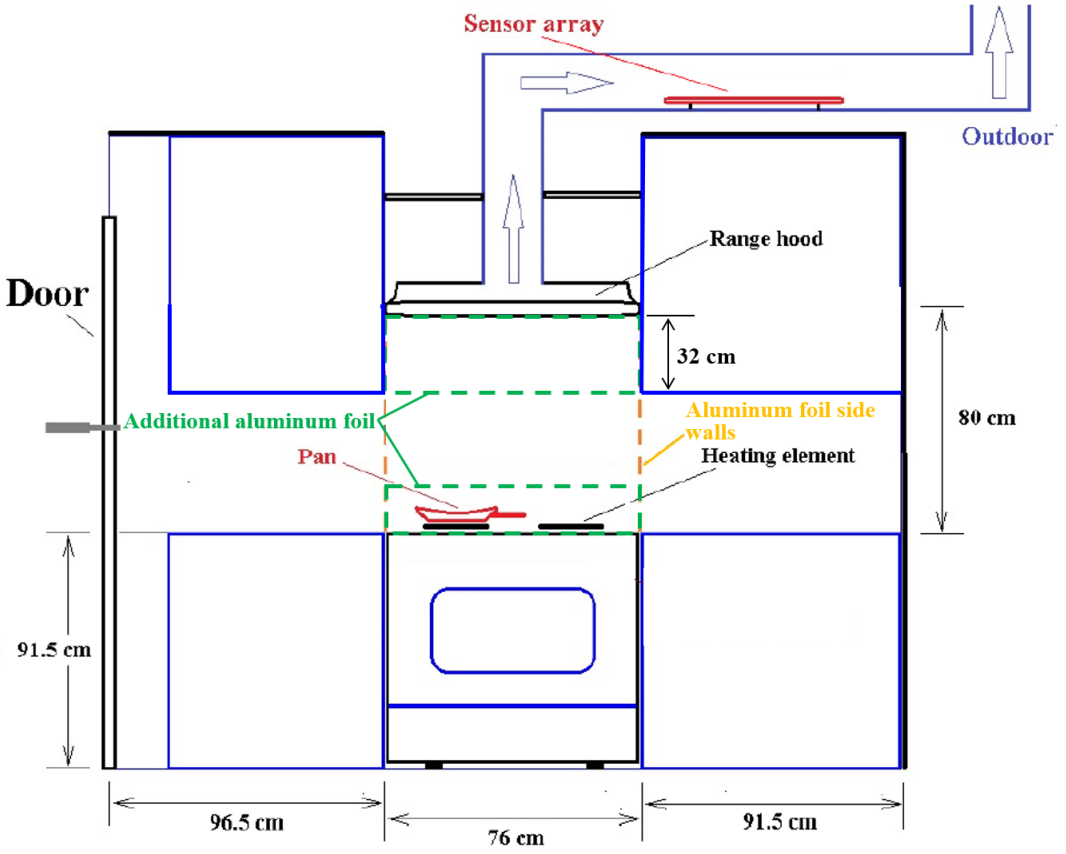

Fig. 1 Two-dimensional schematic of the front of the mock kitchen experimental setup (not to scale).

2 Experimental Methods

Sixty ignition and normal-cooking experiments were conducted in a mock kitchen shown in Figure 1 using either an electric-coil cooktop, gas-fueled cooktop, or electric oven for broiling. There were four different burners used in the cooktop experiments: the small 15 cm diameter electric-coil heating element with a measured power of 1.1 kW, the large 20 cm diameter electric-coil heating element with a measured power of 1.8 kW, the medium gas burner with an estimated heat output of 3.4 kW, and the large gas burner with an estimated heat output of 4 kW.

Sixteen sensors were placed in the exhaust duct where they were exposed to the well-mixed exhaust flow containing gases and particles representative of cooking. The location of the sensors was approximately 3 m downstream of the range hood opening, which was 0.8 m above the cooktop. The sensors monitored various quantities including CO_2, CO, temperature, humidity, smoke, hydrocarbons, alcohols, hydrogen (H_2), natural gas, propane, volatile organic compounds (VOC), and dust/aerosols. Sensor data were acquired at 0.25 Hz. Many of the sensors output a voltage reading, which has not been calibrated to concentration or other measurements. If these sensors are used in further development of a prediction algorithm, the signals should be calibrated.

The exhaust fan was normally set to the highest setting on the range hood. The flow in the exhaust duct (15 cm diameter) was characterized using a bi-directional probe placed in the center of the duct

about 20 diameters downstream of a bend. The typical, average velocity was 3.4 m/s with a standard uncertainty of ± 0.1 m/s. The average velocity varied between experiments with a standard deviation of 0.2 m/s. Using the electric-coil cooktop, the duct temperature increased by an average of 9 °C causing an estimated reduction in duct mass flow of 3 %. For the gas cooktop, the duct temperature increased by an average of 23 °C, which is estimated to reduce the duct mass flow by 7 %. Aluminum foil was added on the sides of the cooktop to reduce the impact of room air currents on the plume flow above the heated pan and reduce transport effects. For Experiments 8 to 15 and 19 to 34, additional aluminum foil, shown in green in Figure 1, was added to the front of the cooktop and exhaust hood to ensure that most of the plume flowed into the hood and past the sensors stationed in the duct.

2.1 Experimental Cooking Scenarios

The cooking scenarios covered a wide range of conditions representative of normal cooking as well as conditions beyond normal cooking, sometimes leading to ignition of the food. The experiments used round, cast iron, aluminum, multi-layered, and stainless-steel pans with diameters of either 20 cm (8 in) or 25 cm (10 in). Typically, one pan of food was heated per experiment, but multiple pans were simultaneously heated on separate burners in a few experiments. In most cases, the smaller burner was used for the 20 cm pan, and the larger burner was used for the 25 cm pan.

The conditions for all 60 experiments are described in Table 1. The foods in the experiments were vegetable oils, butter, water, hamburgers, salmon, bacon, frozen french fries, and chicken. Common vegetable cooking oils in the U.S [9], soybean, canola, olive, sunflower, and corn oils, were tested. In total, 39 of the 60 experiments led to auto-ignition of the food, including cooking oils, salmon, fries, and bacon. Ignition typically occurred 10 min to 15 min after turning on the burner.

Cooking oils and bacon were heated on the highest burner setting until ignition occurred or the sensor signals began to drop and only char remained. The cooking procedure for the hamburgers (80 % lean) was the same as in Cleary [10]. Two hamburgers were also cooked on a broiler pan placed on the top shelf of the oven on the broil setting, according to the UL 217 Cooking Nuisance Smoke Test procedure [11].

The cooking procedures for salmon, chicken and frozen fries were based on the consensus from a variety of recipes. In the salmon cooking procedure, the butter was heated on high for 3 min, the salmon was added and heated on high for 4 min, and the salmon was flipped and cooked on high for 4 min. Following that procedure, unattended cooking was simulated by continuing to cook the salmon at the highest setting. In one case, the salmon eventually ignited. For chicken legs in 200 mL of preheated oil, the burner was set to half of the maximum to maintain a pan temperature of about 200 °C for frying. The chicken legs were flipped four times, every 4 min. For frozen fries, initially 500 mL of canola oil was preheated to 200 °C. After the frozen fries were added, the burner power was adjusted to maintain a pan temperature around 200 °C. After 15 min of cooking, the burner was turned to its highest setting, and the food later ignited.

2.2 Pan Temperature Measurements

In each experiment, pan temperatures were measured at one or more locations using Type-K thermocouples either spot welded or peened to the food side of the pan. The thermocouples showed significant variations in temperature across the pan surface. The standard uncertainty of the Type-K thermocouples was ± 2.2 °C according to the manufacturer. Figure 2 shows calibrated infrared (IR) images of dry, (no oil) cast-iron pans. The images reveal the distribution of temperatures on the small electric coil element and on the large gas burner, which was influenced by pan orientation and geometry. The maximum temperature the camera could monitor was 370 °C, so regions above that temperature are shown as white. The simultaneous, thermocouple measurements that were used to calibrate the IR images are labeled in

Table 1 Experimental Conditions

Number	Ignition	Heating Source	Pan Type	Pan Diameter (cm)	Food & Amount
1	Y	1.1 kW electric coil	cast iron	20	50 mL canola oil
2	Y	1.1 kW electric coil	cast iron	20	50 mL canola oil
3	Y	1.1 kW electric coil	cast iron	20	50 mL canola oil
4	Y	1.1 kW electric coil	cast iron	20	50 mL canola oil
5	Y	1.1 kW electric coil	cast iron	20	50 mL canola oil
6	Y	1.1 kW electric coil	cast iron	20	50 mL canola oil
7	Y	1.1 kW electric coil	cast iron	20	50 mL canola oil
8	Y	1.1 kW electric coil	cast iron	20	50 mL canola oil
9	Y	1.1 kW electric coil	cast iron	20	100 mL canola oil
10	Y	1.1 kW electric coil	aluminum	20	50 mL canola oil
11	Y	1.1 kW electric coil	multi-layered	20	50 mL canola oil
12	Y	1.1 kW electric coil	stainless steel	20	50 mL canola oil
13	Y	1.1 kW electric coil	cast iron	20	200 mL canola oil
14	Y	1.8 kW electric coil	cast iron	20	50 mL canola oil
15	Y	1.8 kW electric coil	cast iron	25	100 mL canola oil
16	N	1.1 kW electric coil	aluminum	20	50 mL corn oil
17	Y	1.1 kW electric coil	aluminum	20	50 mL corn oil
18	Y	1.1 kW electric coil	cast iron	20	50 mL corn oil
19	Y	1.8 kW electric coil	cast iron	25	100 mL corn oil
20	Y	1.1 kW electric coil	cast iron	20	50 mL corn oil
21	Y	1.1 kW electric coil	cast iron	20	50 mL soybean oil
22	Y	1.8 kW electric coil	cast iron	25	100 mL soybean oil
23	Y	1.1 kW electric coil	cast iron	20	50 mL olive oil
24	Y	1.8 kW electric coil	cast iron	25	100 mL olive oil
25	Y	1.8 kW electric coil	cast iron	25	100 mL sunflower oil
26	Y	1.1 kW electric coil	cast iron	20	50 mL sunflower oil
27	Y	1.1 kW electric coil	cast iron	20	46 g butter
28	N	electric oven	broiler pan	N/A	460 g (1 lb) of hamburgers (2)
29	N	1.1 kW electric coil	cast iron	20	230 g (0.5 lb) hamburger (1)
30	N	1.8 kW electric coil	cast iron	25	460 g (1 lb) of hamburgers (2)
31	Y	1.1 kW electric coil	cast iron	20	227 g (8 oz) salmon & 42.5 g butter
32	N	1.8 kW electric coil	cast iron	25	454 g (16 oz) salmon & 85.1 g butter
33	N	1.1 kW electric coil	cast iron	20	50 mL water
34	N	1.8 kW electric coil	none	N/A	N/A
35	Y	1.1 kW electric coil	cast iron	20	50 mL canola oil & 2 L water on separate burners
36	Y	1.1 kW electric coil	cast iron	20	50 mL canola oil
37	N	1.1 kW electric coil	cast iron	20	50 mL canola oil
38	N	1.1 kW electric coil	aluminum	20	50 mL canola oil
39	N	1.1 kW & 1.8 kW electric coil	cast iron & aluminum	20	50 mL canola oil in each pan
40	N	1.1 kW electric coil	cast iron	20	50 mL canola oil
41	N	electric oven	broiler pan	N/A	460 g of hamburgers (2)
42	N	1.1 kW electric coil	cast iron	20	227 g (8 oz) salmon & 45.4 g butter
43	N	1.1 kW electric coil	cast iron	20	282 g chicken legs (2) & 200 mL canola oil
44	Y	1.8 kW electric coil	cast iron	25	223 g frozen french fries & 500 mL canola oil
45	N	1.8 kW electric coil	cast iron	25	220 g bacon (8 slices)
46	Y	1.1 kW electric coil	cast iron	20	110 g bacon (4 slices)
47	N	1.8 kW electric coil	cast iron	25	460 g (1 lb) of hamburgers (2)
48	Y	1.1 kW & 1.8 kW electric coil	cast iron	20 & 25	50 mL & 100 mL canola oil in separate pans
49	Y	1.1 kW & 1.8 kW electric coil	cast iron	20 & 25	50 mL & 100 mL canola oil in separate pans
50	Y	1.1 kW & 1.8 kW electric coil	cast iron	20 & 25	50 mL & 100 mL olive oil in separate pans
51	Y	1.1 kW electric coil	cast iron	20	50 mL canola oil
52	N	4 kW methane gas	none	N/A	N/A
53	N	3.4 kW methane gas	cast iron	20	50 mL canola oil
54	Y	4 kW methane gas	cast iron	25	100 mL canola oil
55	N	4 kW methane gas	cast iron	25	N/A
56	Y	4 kW methane gas	cast iron	25	100 mL canola oil
57	Y	4 kW methane gas	cast iron	20	50 mL canola oil
58	Y	4 kW methane gas	cast iron	25	100 mL canola oil
59	N	4 kW methane gas	none	N/A	N/A
60	N	3.4 kW & 4 kW methane gas	cast iron	20 & 25	50 mL & 100 mL canola oil in separate pans

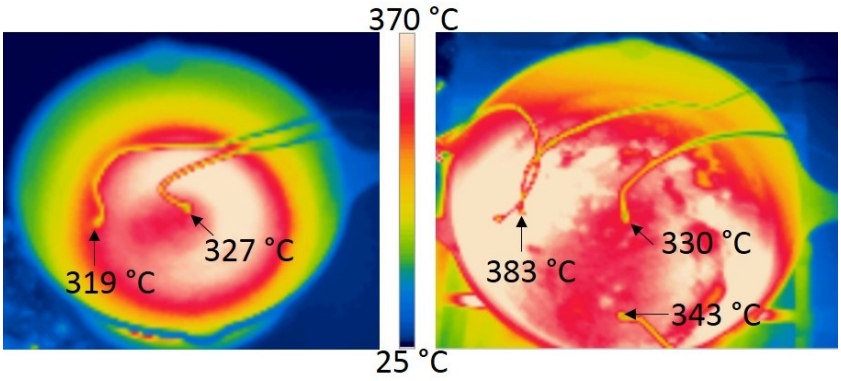

Fig. 2 IR images showing the distribution of surface temperature on a 20 cm diameter cast iron pan heated by the small electric coil heating element (left) and the large gas burner (right).

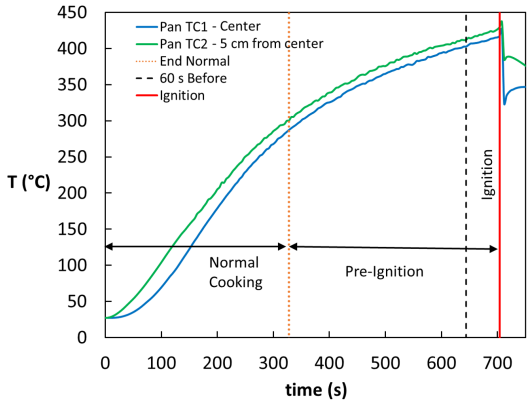

Fig. 3 Pan surface temperatures and cooking regimes for an experiment leading to ignition of 50 mL of canola oil, Experiment 8.

the figure. From the thermocouple calibrations, the pan emissivity ranged from 0.88 to 0.96, depending on the experiment. The uncertainty in the IR temperatures was ± 8 °C. Figure 3 shows the thermocouple measurements on the pan surface during Experiment 8, which ended with the ignition of canola oil. These figures demonstrate that temperature variation across the pan's bottom surface was as large as 50 °C.

Figure 3 shows that the temperature at the center of the pan lagged temperatures measured toward the edge of the pan throughout the experiment until ignition. For some experiments, there was only one thermocouple in the pan, measuring the center temperature. Because ignition is related to the hottest pan temperatures, the peak pan temperatures were estimated in experiments when only the center pan temperature was measured. The estimates were based on linear regressions between the thermocouple readings at the pan center and at the edge locations: 5 cm from the center in the 20 cm diameter cast iron pan, and 6 cm or 7.5 cm from the center in the 25 cm diameter cast iron pan. The linear regression relationships for the edge temperatures are shown in Table 2 as a function of center temperature for similar experiments (same pan size and burner size).

The average pan temperature at the time of ignition for all the experiments was 429 °C (standard deviation of 25 °C). For the electric-coil experiments, the pan temperature at the time of ignition was between 403 °C and 483 °C, consistent with previous studies [12]. For the gas cooktop, the ignition temperatures of the pan were lower, between 371 °C and 382 °C. The gas cooktop also took much longer

Table 2 Relationships Between Pan Thermocouple Temperatures

Experiment Type	Linear Regression	R^2
Electric coil, cast iron 20 cm pan, small burner	$T_{5cm} = 0.972\ T_{center} + 23\ °C$	0.99
Electric coil, cast iron 25 cm pan, large burner	$T_{6cm} = 1.07\ T_{center} + 16\ °C$	1.00
Methane, cast iron 25 cm pan, large burner	$T_{7.5cm} = 0.967\ T_{center} + 31\ °C$	0.99

to ignite. The average time to ignition was 536 s for the 25 cm pan on the large, electric-coil burner and 1104 s for the 25 cm pan on the large gas burner. In general the temperature rise for the pans on the gas cooktop were slower than on the electric-coil cooktop. In addition, ignition was not observed using the medium, gas burner; ignition occurred only when the pan was heated on the large, gas burner. Heating a pan represents a complex set of heat transfer processes involving radiation, convection and conduction, and the burner and pan configurations play an important role.

2.3 Defining Normal Cooking

To develop an algorithm that predicts ignition, normal cooking must be defined. This is because sensor performance involves not only quantifying the rate of missed ignitions, but also the rate of false alarms. A missed ignition means the algorithm would not have predicted ignition with enough time to intervene and prevent ignition. To evaluate the algorithms the amount of necessary lead time is defined, considering the thermal lag of the cooktop and burner-pan system. Processing lag associated with the algorithm itself is not considered; the algorithm is assumed to act immediately based on the signals received from the sensors. Previous work on an electric-coil cooktop suggests that a period of 60 s before ignition is enough time to intervene and prevent the ignition [6] despite potential thermal lag leading to additional temperature rise in the system. A 60 s period of time was supported by results from Experiments 37 to 39, where the power to the electric coil cooktop was cut after about 5 min of heating of the oil on maximum power. The pan temperature continued to increase after the burners were turned off in all three experiments, for 48 s in Exp. 37, 16 s in Exp. 38, and 60 s in Exp. 39. A false alarm means the algorithm predicts that ignition is imminent, but the conditions are that of normal cooking, and ignition is not likely.

Figure 3 illustrates three periods of a typical experiment: normal cooking, pre-ignition, and ignition. Initially, all experiments start as normal cooking. At some point, the conditions exceed some reasonable temperature-based or time-based limit and transition to "pre-ignition." Therefore, any condition that is not defined as normal cooking is labeled as pre-ignition, regardless of whether or not ignition eventually occurs in the experiment. This is because the conditions during pre-ignition are considered beyond the requirements of normal cooking and potentially hazardous. Such conditions are accompanied by severely burned or charred food and copious amounts of aerosol. Since there is no experiment in which normal cooking overlapped with the period 60 s before ignition, these definitions make it possible for algorithms to predict ignition without interfering with normal cooking.

While the definition of the ignition period is straightforward, establishing reasonable limits of normal cooking requires more nuance. The limits of normal cooking are based on either a maximum pan temperature, a safe food temperature, or the duration of cooking at an approximate pan temperature. For example, because the thickness of the vegetable oils and butter was thin (typically 3 mm), it was assumed that pan temperature was a good indication of the oil temperature. Additionally, steady-state heat transfer was confirmed with measurements of the oil mass loss for the most common cooking case of 50 mL of oil in a 20 cm cast iron pan on the 25 cm electric coil burner. Following the initial 35 s of transient heating, the mass loss rate was approximately constant at 0.01 g/s until ignition. When cooking foods such as meat, the pan temperature could be much hotter than the food, and food temperature was a better indicator of ignition potential than pan temperature. In defining normal cooking for meats, the USDA

safe minimum internal temperatures for chicken (74 °C), fish (63 °C), and ground beef (71 °C) [13] were used.

The end of normal cooking for all types of oils and butter was defined when the pan temperature reached 300 °C. When deep-frying, it is recommended to keep oils below their smoke point, and the highest oil smoke points are around 230 °C [14]. Therefore, a limit of 300 °C allowed significantly more heating than recommended, while being well below oil ignition temperatures. For bacon, a USDA fact sheet states, "It's very difficult to determine the temperature of a thin piece of meat such as bacon, but if cooked crisp, it should have reached a safe temperature." [15] Instead of relying on a crispness determination, we treated bacon like oils, and the end of normal cooking was when the pan temperature reached 300 °C. This was reasonable since bacon is very high in fat, and liquid fat quickly coats the pan like vegetable oil. Photos taken at a pan temperature of 300 °C showed that the bacon had already begun to blacken. Some bacon experiments led to ignition.

For chicken legs in 200 mL of preheated oil, the burner was set to medium power to maintain a pan temperature of about 200 °C for frying. The chicken legs were flipped every 4 min for a total cooking time of 18.5 min, which was 10 % longer than the time it took for the thermocouple inserted in the middle of the meat to reach 74 °C. This time was defined as the end of normal cooking, and the internal chicken temperature was 80 °C. For salmon fried in butter on high power for 4 min on each side, the thermocouples inside the meat did not show a steady increase in temperature. In most cases, the meat temperature exceeded 63 °C at least momentarily before the end of the 8 min cooking period, which was taken as the end of normal cooking.

For hamburgers, the end of the frying procedure used by Cleary [10] was about 10 % longer than the time for the temperatures in the middle of the hamburgers to reach 71 °C. At the end of this procedure, the meat temperature was about 77 °C, which is an indication of well-done beef [16]. Therefore, the end of the frying-hamburger procedure was defined as the end of normal cooking. For broiling hamburgers, the UL 217 Cooking Nuisance Smoke Test [11] specifies 25 min of broiling. However, in our experiments, adding an additional 10 % to the time when the hamburgers reached 71 °C, was less than 18 min (1122 s). Therefore, this was defined as the end of normal cooking, and at this time the meat temperature was 82 °C.

For frozen fries in 500 mL of preheated oil, the burner power was adjusted periodically to maintain a pan temperature around 200 °C, like was done for the experiments cooking chicken legs. There is no recommended safe temperature for fries, so the end of normal cooking was defined as 15 min of frying and when the color of the fries had turned medium brown. After the end of normal cooking, the burner power was turned to high and the fries and oil later ignited.

3 Sensor Analysis

Each sensor signal was characterized by its unique profile with its absolute value and slope varying in time. Eleven of the sensor signals tended to increase in time as ignition approached, as shown in Figure 4 (Experiment 8) and Figure 5 (Experiment 57). Not plotted are the CO_2, humidity, and duct temperature sensors, which were less responsive before ignition, and typically increased sharply just after ignition. The figure legend indicates the detection target of the sensor. HCs means hydrocarbons such as butane, propane, and methane, and IAQ means indoor air quality. A sensor may respond to quantities other than those indicated by its label, such as the dust sensor, which operates using light scattering and responds to both dust particles and cooking aerosols. The average background signals of the 11 responsive sensors were subtracted from the raw, signal outputs. The complete set of sensor data for all experiments is reported in [17].

Figures 4 and 5 plot the signals of the 11 responsive sensors for canola-oil experiments on an electric-coil burner and a gas burner, respectively. For clarity, the signals in Figures 4 and 5 are normalized by

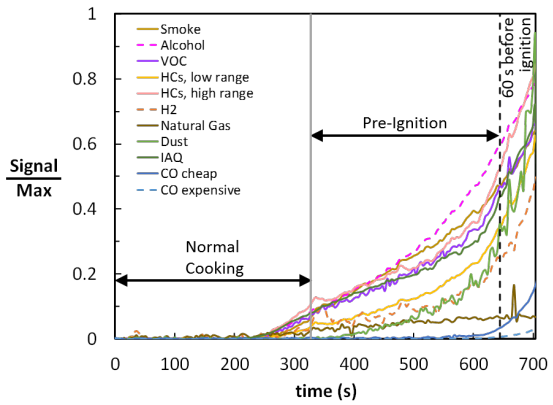

Fig. 4 Sensor signals (background subtracted and normalized by sensor peak) and cooking regimes for an experiment leading to ignition of canola oil in a cast iron pan on an electric-coil burner, Experiment 8.

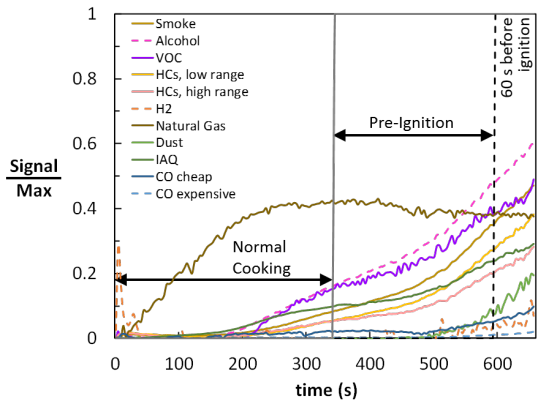

Fig. 5 Sensor signals (background subtracted and normalized by sensor peak) and cooking regimes for an experiment leading to ignition of canola oil in a cast iron pan on a gas burner, Experiment 57.

the maximum value recorded from that sensor over all experiments. In both figures, ignition occurred at the maximum time shown on the graph, and the ignition period of 60 s before ignition is marked. The regimes of normal cooking and pre-ignition are also shown, with the transition occurring when the pan temperature exceeded 300 °C. The most noticeable differences in the sensor responses between the experiments are the responses of the natural gas sensor and the generally lower signals for the gas burner experiment. Reduced sensor signals for the experiments with the gas cooktop compared to electric coil was a consistent trend across the experiments.

Sensor signals and their ratios were evaluated across all experiments to determine if a threshold value could be selected to both prevent ignition and ignore normal-cooking conditions. Machine learning was also used to classify sensor data as representing normal cooking or pre-ignition conditions, and a similar performance metric was used.

3.1 Threshold Analysis

A threshold value of a sensor or sensor ratio could potentially miss ignitions as well as trigger false alarms. We considered the most conservative sensor or ratio threshold, which is the minimum value obtained at

least 60 s before all ignitions. The false alarm rate (FAR) to evaluate the threshold performance, defined in Equation 1, was the ratio of the number of experiments with a false alarm to the total number of experiments. The FAR can also be described as the false positive rate.

$$\text{FAR} = \frac{\text{false alarms}}{\text{total \# experiments}} = \frac{\text{\# exp. exceeding threshold during normal cooking}}{60} \quad (1)$$

In addition to investigating the performance of thresholds of individual sensor values as a criteria to prevent cooktop ignition and minimize false alarms, the ratios between sensor values were also considered. Carbon dioxide (mole fraction), duct temperature (K), and humidity (mole fraction of water) signals were used in the denominator of ratios. These signals did not include background subtraction to avoid dividing by zero because the values during the experiment were similar to the background.

3.2 Neural-Network Analysis

The sensor signals were also used to train a multi-layer perceptron that can differentiate between normal cooking and pre-ignition conditions. A four-layer neural-network architecture was used with one input layer, two hidden layers, and one output layer. The two hidden layers, with 64 neurons and 32 neurons, respectively, were activated with a rectified linear unit (ReLU) activation function. The numbers of hidden layers and neurons were selected based on initial testing for accuracy and efficiency. The initial testing was performed for neural networks trained on 28 experiments and tested on five experiments. Beginning with one hidden layer of eight neurons, neurons were added, and then hidden layers, until there was no longer a significant improvement in performance. The ReLU activation function was used for its numerical performance in engineering applications. For the output, a sigmoid activation function was used because it gives a probability ranging from 0 to 1. The maximum number of epochs or iterations was set to 300, and the iterations were stopped if the validation accuracy did not improve for five consecutive iterations.

Each time point was classified individually with a label assigned as "0" during the normal cooking window and "1" during the pre-ignition period. The analysis considered over 12 800 time points in the 60 experiments. A cross-validation method, where the neural-network model was trained using the data from 59 experiments (training set) and then tested on the last experiment (testing set), was used. This process was repeated 60 times until each experiment was excluded from the training and used once as the test set. Each iteration of training and testing was done on a newly created neural network. The output for each time point in the test experiment, a value between 0 and 1, was the model prediction for the probability of pre-ignition for that time. The values were converted to 0 or 1 using thresholds of 0.5, 0.8, 0.9 or 0.98 to compare the model predictions to the binary labels from the experiment.

There were 35 total neural-network models developed, including 28 unique cases that used different sets of training data and seven repeat cases, to characterize repeatability of the model development. The baseline case used all 11 sensor data sets as the input training data. Eleven cases were based on only a single sensor as training input. Finally, 16 unique pairs of sensors were used as input data for additional cases, which are listed in Table 3. The pairs were selected from the individual sensors with the best threshold or machine learning performance and from the sensors included in the ratios with the best performance. The repeated cases were the baseline case, three single sensor cases (using the VOC, IAQ, and smoke sensors), and the three best performing cases using sensor pairs, noted in Table 3.

The overall performance was evaluated by quantifying the rate of false alarms and the rate of missed ignitions on a per-experiment basis. The rate of false alarms (FAR) was the same as defined in Equation 1, with a false alarm defined as an experiment with any wrongly predicted values above the threshold within the normal cooking window. A missed ignition was an experiment where ignition occurred, but the prediction value did not reach the threshold at any time up to the start of the ignition window (60 s

Table 3 Neural-Network Model Cases Based on Pairs of Sensor Signals

Sensor Input Data
VOC & Duct Temp.
VOC & Humidity
VOC & IAQ
VOC & Dust[1]
VOC & CO expensive[1]
VOC & CO cheap[1]
IAQ & Duct Temp.
IAQ & Humidity
IAQ & Dust
IAQ & Smoke
IAQ & CO expensive
IAQ & CO cheap
Dust & Duct Temp.
Dust & CO expensive
Dust & CO cheap
Smoke & CO expensive

[1] repeated case

before ignition). A practical implication of this definition is that if a sensor caused a false alarm in an experiment, the same experiment could not be counted as a missed ignition for that sensor. To calculate the missed ignition rate (MIR), the number of missed ignitions was divided by the number of experiments in which ignition was observed. The MIR can also be described as the false negative rate.

$$\text{MIR} = \frac{\text{missed ignitions}}{\text{\# ignition experiments}} = \frac{\text{\# exp. not reaching threshold before ignition window}}{39} \tag{2}$$

4 Results and Discussion

4.1 Threshold Results

For individual sensors, the optimal threshold values such that no ignitions are missed are reported in Table 4 along with the operating principle of each sensor. With the exception of the expensive CO sensor and the IAQ sensor, most of the thresholds are reported as measured voltages because the sensors have not been calibrated. The output of the IAQ sensor corresponds to the equivalent mole fraction of CO_2 $\times 10^{-6}$ (PPM), according to a calibration from the manufacturer. The threshold's estimated uncertainty is determined from the range in the signal during the background measurement period of one experiment, and reported as a percentage of the optimal threshold. The performance of the threshold with no missed ignitions is reported as the FAR. Also shown is the maximum FAR that would have occurred if the threshold was decreased by the uncertainty and the maximum missed ignition rate that would have occurred if the threshold was increased by the uncertainty.

The best performance is for the VOC sensor with a 0.02 false alarm rate, or one false alarm in 60 experiments. The false alarm occurred about two minutes before the end of normal cooking in Experiment 47. This was one of the experiments in which frying hamburgers were cooking on a 25 cm cast-iron pan on the large, electric-coil burner. At that time, the thermocouples inside the hamburgers were both 68 °C, which is just below the safe temperature for ground beef (71 °C), but still within our definition of normal cooking. However, when taking into account the threshold uncertainties, the VOC sensor would have a non-zero missed ignition rate (miss one ignition), while the IAQ and dust sensors would not miss any ignitions.

Table 4 Optimal Thresholds of Individual Sensors and Their Performance

Sensor	Threshold	Units	Estimated Threshold Uncert.	False Alarm Rate (FAR)	FAR w/ Threshold Decrease	Missed Ignition Rate (MIR) w/ Threshold Increase	Operating Principle
VOC	0.57	V	3 %	0.02	0.02	0.03	metal oxide semiconductor
IAQ	12 300	$\times 10^{-6}$ (mole fraction)	1 %	0.05	0.07	0	metal oxide semiconductor
Dust	0.20	V	14 %	0.08	0.12	0	light scattering
Alcohol	0.99	V	1 %	0.10	0.12	0.03	electrochemical
Smoke	0.49	V	11 %	0.22	0.28	0.03	electrochemical
CO expensive	4.7	$\times 10^{-6}$ (mole fraction)	64 %	0.22	0.71	0.03	electrochemical
CO cheap	0.0088	V	156 %	0.23	1.00	0.21	electrochemical
HCs, low range	0.23	V	14 %	0.23	0.27	0.03	electrochemical
HCs, high range	0.17	V	25 %	0.38	0.48	0.03	electrochemical
H_2	0.0083	V	157 %	0.47	1.00	0.21	electrochemical
Natural gas	0.0058	V	130 %	0.92	1.00	0.13	electrochemical

The estimated relative uncertainties of some of the sensor thresholds were substantial. This was the case for both CO sensors, the H_2 sensor, and the natural gas sensor. For these sensors, the threshold for detection was on the same order or less than the signal variation. The two different CO sensors perform similarly despite the differences in output format and price. However, the two CO sensors had quite different threshold uncertainties, with the uncertainty for the cheaper CO sensor much higher than the expensive CO sensor. The CO, H_2, and natural gas sensors all perform much worse when considering their threshold uncertainties, with significant missed ignition rates or high false alarm rates. Using these sensors alone would likely result in poor performance in practice due to the inevitable signal variations from different sensors and different cooking conditions.

Figure 6 shows the performance of the eight individual sensors with the lowest false alarm rates as well as their ratios with duct temperature, humidity, and CO_2. The lowest FAR was with the VOC sensor alone and in a ratio with duct temperature. These performed significantly better than all the other sensors or ratios of sensors by a factor of 2 to 15. The ratios of sensors with duct temperature have similar performance to the sensor alone, while the ratios with humidity or with CO_2 tend to perform the same or worse than the sensor alone. One exception is the ratio of the expensive CO sensor to CO_2, which is slightly better than the CO sensor alone. The most significant improvement occurs for the ratio of the low range hydrocarbon sensor to humidity, with the false alarm rate for the ratio falling to 0.15 from the hydrocarbon sensor alone at 0.23. The ratio of the low-range, hydrocarbon sensor to the duct temperature is also slightly lower than the hydrocarbon sensor alone.

4.2 Neural-Network Results

An example output of the neural-network analysis is given in Figure 7, which shows the specific predictions for one experiment from one model case. The labels for pre-ignition and ignition from Experiment 24 are shown as well as the prediction of pre-ignition from one of the baseline models (based on 11 sensors). In this case, use of any of the four prediction thresholds (0.5, 0.8, 0.9, 0.98) results in detection well ahead of the ignition window, which begins 60 s before ignition (red symbols). However, both the 0.5 and 0.8 thresholds are reached before the end of normal cooking, and therefore would be considered a false alarm. Note that once a threshold is reached, that threshold line continues to be 1 even if the prediction

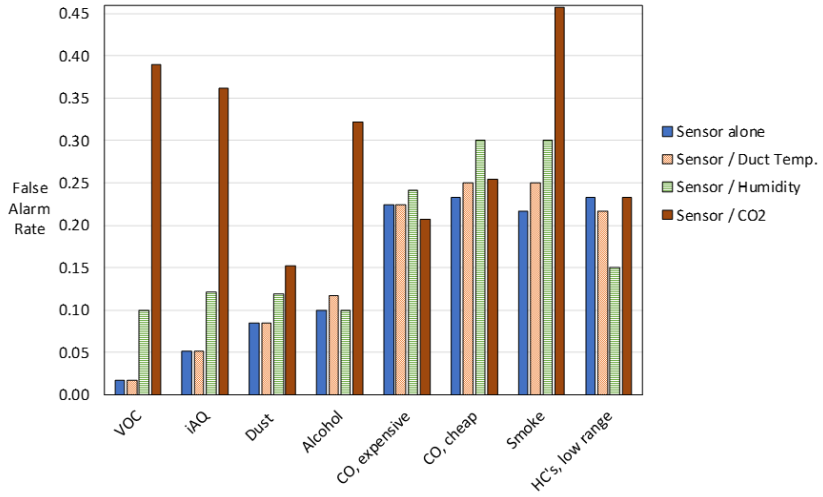

Fig. 6 Threshold false alarm rates of the eight top performing individual sensors and of their ratios with duct temperature, humidity, and CO_2.

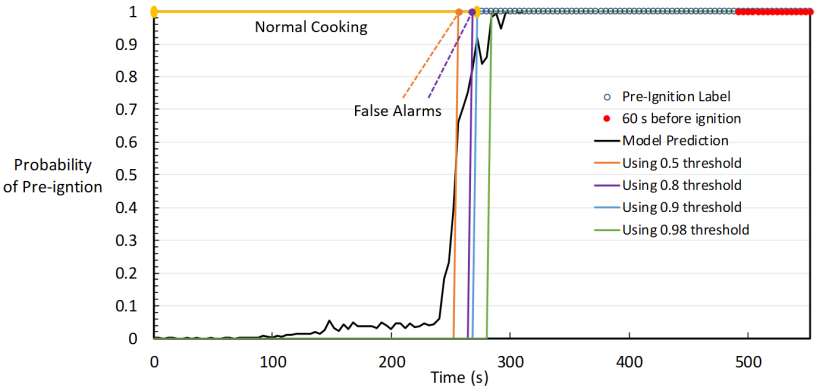

Fig. 7 Baseline (11 sensor) neural-network model predictions and results using different thresholds for Experiment 24.

curve later drops below the threshold. This is to reflect the functionality of the system in a real application, where an intervention to the hazardous situation would only need to be triggered once.

The false alarm rates and missed ignition rates are plotted in Figure 8 as a function of the prediction threshold for three different neural-network models. False alarm rates are represented by filled symbols, and missed ignition rates are in open symbols. In blue circles, are the rates for the two model cases, both trained with only the VOC sensor data. The rates for the models trained with data from the smoke sensor are in red. The baseline models trained with all 11 sensors are in black. The performance of repeat model cases differed by at most 0.07 (4/60 experiments) for FAR and at most 0.03 (1/39 experiments) for missed ignition rate. The lowest false alarm rate with zero missed ignitions is also labeled for the models based on the VOC sensor, the smoke sensor, and all 11 sensors (baseline).

In all cases, as the prediction threshold increased, the false alarm rate decreased. The missed ignition rates were typically lower than the false alarm rates because the neural network was trained to predict the pre-ignition window, which began well before the ignition window. All missed ignition rates using a prediction threshold of 0.5 were zero. However, the trends of the missed ignition rates differed as the

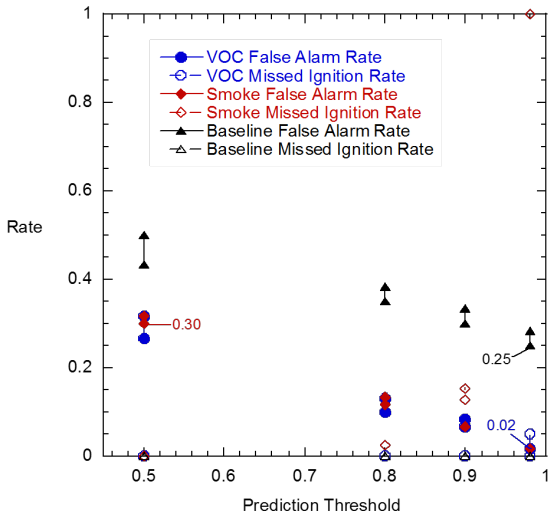

Fig. 8 Neural-network model false alarm rates and missed ignition rates as a function of prediction threshold, using VOC sensor, smoke sensor, and 11 sensors as input (baseline).

Table 5 Best Performing Neural-Network Model Cases with Missed Ignition Rates of Zero

Sensor Input Data	Prediction Threshold	False Alarm Rate
VOC[1]	0.98, 0.9	0.02, 0.08
VOC & CO cheap[1]	0.98, 0.9	0.02, 0.08
VOC & CO expensive[1]	0.98, 0.98	0.03, 0.05
VOC & Dust[1]	0.98, 0.98	0.05, 0.05
VOC & Duct Temp.	0.9	0.07
IAQ[1]	0.8, 0.8	0.09, 0.09
IAQ & CO expensive	0.8	0.10
VOC & IAQ	0.9	0.10
Dust	0.8	0.12
Dust & CO expensive	0.8	0.12
Dust & CO cheap	0.8	0.14
IAQ & Dust	0.8	0.14
IAQ & Duct Temp.	0.8	0.14

[1] repeated case

prediction threshold increased. The models based on the VOC sensor had zero missed ignitions until the threshold was 0.98, when the missed ignition rate of one repeat was 0.05. The models based on the smoke sensor started having missed ignitions for a threshold of 0.8, and the missed ignition rate increased to 1 (missing all ignitions) by the 0.98 threshold. The baseline models had zero missed ignitions for all prediction thresholds tested.

Table 5 summarizes the best performing models from the neural-network analysis. In order to compare the performance of the neural-network models to the performance using sensor thresholds, only cases with missed ignition rates of zero are listed. For each case, the highest threshold (out of 0.5, 0.8, 0.9 and 0.98), that still had a zero missed ignition rate, is used to determine the false alarm rate in Table 5. In other words, the lowest false alarm rate that did not miss any ignitions is reported for the model. Repeat model cases for the VOC sensor, the IAQ sensor, and three sensor pairs are reported as well.

The best performing neural-network models were based on the VOC sensor alone and on the combination of the VOC and cheap CO sensors. Their best performance matched the 0.02 FAR, using a threshold

of 0.57 V for the VOC sensor signal or a threshold of 0.0019 V/K for the ratio of the VOC sensor to the duct temperature. The one false alarm for the neural-network models would have occurred at the same time as the VOC sensor exceeded the 0.57 V threshold in Experiment 78. The VOC and expensive CO sensor neural-network model also performed well with a 0.03 false alarm rate (2 out of 60 experiments).

The best performing sensors in the neural-network analysis are the VOC, IAQ and dust sensors, one of which is included in each of the top performing model cases in Table 5. These are the same three sensors with the best signal threshold performance in Table 4. The false alarm rates from the neural-network models based on these individual sensors are within 0.04 of the false alarm rates based on thresholds of the individual signals. For the IAQ and dust sensors, the neural-network models have two additional false alarms compared to the signal threshold, while the VOC neural-network model has the same number.

Some neural-network models trained with multiple sensors had similar or improved performance over the models trained with only one sensor. The models using the CO sensors individually did not perform well and are not listed in Table 5 because they had missed ignition rates of 0.05 and higher. However, the CO sensors usually complemented other sensors. In the pairing with the VOC sensor and either CO sensor, the model had similar or improved performance compared to the single sensors. Pairing the VOC sensor with the dust sensor was also similar or improved performance compared to the individual sensors. The baseline model using all 11 sensors performed worse than many of the models based on pairs or individual sensors (false alarm rate of 0.25). The baseline model performance was probably negatively affected by including input data from the poorest performing sensors, two of which had individual sensor models with false alarm rates above 0.5 (H_2 and natural gas sensors).

5 Conclusions

A set of cooking experiments was designed to investigate the feasibility of creating a robust and reliable model to detect pre-ignition conditions for a kitchen cooktop with enough time to prevent food ignition. Sixteen off-the-shelf sensors collected data in the exhaust duct above the cooktop, and the sensor data were analyzed using thresholds for the signals and signal ratios and using machine learning models. A precise and consistent definition of normal cooking versus pre-ignition was required to evaluate model performance.

Both signal threshold analysis and machine learning analysis were in complete agreement identifying the most effective individual sensors at providing early detection of impending ignition. The three best performing sensors were VOC, IAQ, and dust, and both analyses predicted similar rates of false alarms for zero missed ignitions. The VOC sensor appeared to be the most effective sensor, but when considering the estimated uncertainty in the VOC signal, the VOC threshold could have a missed ignition rate of 0.03. Although the IAQ and dust sensors had slightly greater false alarm rates, they would still have zero missed ignitions after applying an estimate for the realistic variation in their thresholds. These three sensors all had a consistent response to the copious amounts of aerosol released before ignition, which likely include volatile organic compounds and smoke. Both the VOC and IAQ sensor manufacturer descriptions mention sensitivity to volatile organic compounds and cooking odors, while the VOC, IAQ and dust sensors all note sensitivity to smoke. Further investigation into the chemical and physical characteristics of pre-ignition cooking aerosols would be beneficial.

The combined information from multiple sensors was evaluated by both threshold analysis and machine learning analysis. In the threshold analysis, some sensor ratios performed as well as or better than the individual sensor values used in the ratios, but none of the ratios performed better than the VOC sensor threshold. In the machine learning analysis, multiple sensors were used to train the baseline model (11 sensors) and models based on pairs of sensors. While the baseline model had a 0.25 false alarm rate, it did not miss any ignitions. The model using the VOC sensor paired with both CO sensors performed as well as the VOC alone, and the model using the VOC and dust sensors performed similarly well. When

two sensors are used to train the neural network, it can learn from the ratio of the signals as well as less intuitive relationships between the signals that correlate well with the classification label. With additional testing scenarios and repeat measurements, models using more than one sensor might be more robust, with less false alarms, because more information is available for the model to make the prediction. Finally, future studies should also investigate the effect of sensor location on the system performance and durability.

References

1. M. Ahrens, Home Fires Involving Cooking Equipment, National Fire Protection Association, Quincy, MA (2017)
2. Underwriter's Laboratory, Northbrook, IL. UL 858, Standard for Household Electric Ranges (2014). URL https://standardscatalog.ul.com/standards/en/standard_858_16
3. D.T. Gottuk, M.J. Peatross, R.J. Roby, C.L. Beyler, Advanced fire detection using multi-signature alarm algorithms, Fire Safety Journal **37**(4), 381 (2002). DOI 10.1016/S0379-7112(01)00057-1. URL http://linkinghub.elsevier.com/retrieve/pii/S0379711201000571
4. L.A. Cestari, C. Worrell, J.A. Milke, Advanced fire detection algorithms using data from the home smoke detector project, Fire Safety Journal **40**(1), 1 (2005). DOI 10.1016/j.firesaf.2004.07.004. URL http://linkinghub.elsevier.com/retrieve/pii/S0379711204000682
5. D.T. Gottuk, M.T. Wright, J.T. Wong, H.V. Pham, S.L. Rose-Pehrson, S. Hart, M. Hammond, F.W. Williams, P.A. Tatem, T.T. Street, Prototype Early Warning Fire Detection System: Test Series 4 Results. Interim Report NRL/MR/6180–02-8602, Naval Research Laboratory (2002)
6. E.L. Johnsson, Study of Technology for Detecting Pre-Ignition Conditions of Cooking-Related Fires Associated with Electric and Gas Ranges and Cooktops, Final Report. NIST Internal Report NISTIR 5950, National Institute of Standards & Technology, Gaithersburg, MD (1998)
7. E. Johnsson, M. Zarzecki, in *16th International Conference on Automatic Fire Detection (AUBE '17) & Suppression, Detection and Signaling Research and Applications Conference (SUPDET 2017)* (2017)
8. A. Jain, P. Nyati, N. Nuwal, A. Ansari, C. Ghoroi, P. Ghandi, Pre-Detection of Kitchen Fires due to Auto-Ignition of Cooking Oil and LPG Leakage in Indian Kitchens, Fire Safety Science **11**, 1285 (2014). DOI 10.3801/IAFSS.FSS.11-1285. URL http://www.iafss.org/publications/fss/11/1285
9. M. Ash, Edible fats and oils: U.S. Supply and disappearance, 2002/03-2015/16. Tech. Rep. 89002, Economic Research Service, United States Department of Agriculture (2016). URL http://usda.mannlib.cornell.edu/MannUsda/viewDocumentInfo.do?documentID=1290
10. T.G. Cleary, A study on the performance of current smoke alarms to the new fire and nuisance tests prescribed in ANSI/UL 217-2015. Tech. Rep. NIST TN 1947, National Institute of Standards and Technology, Gaithersburg, MD (2016). DOI 10.6028/NIST.TN.1947. URL http://nvlpubs.nist.gov/nistpubs/TechnicalNotes/NIST.TN.1947.pdf
11. Underwriter's Laboratory, Northbrook, IL. UL/ANSI 217standard for Safety Smoke Alarms (2015). URL https://standardscatalog.ul.com/standards/en/standard_217_8
12. J.B. Dinaburg, D.T. Gottuk, Development of Standardized Cooking Fires for Evaluation of Prevention Technologies: Data Analysis. Tech. Rep. NIST GCR 15-917-36, National Institute of Standards and Technology (2014). DOI 10.6028/NIST.GCR.15-917-36. URL https://nvlpubs.nist.gov/nistpubs/gcr/2015/NIST.GCR.15-917-36.pdf
13. Safe Minimum Internal Temperature Chart. Tech. rep., United States Department of Agriculture, Food Safety and Inspection Service (2019). URL https://www.fsis.usda.gov/safetempchart
14. Deep Fat Frying and Food Safety. Tech. rep., United States Department of Agriculture, Food Safety and Inspection Service (2013). URL https://www.fsis.usda.gov/wps/portal/fsis/topics/food-safety-education/get-answers/food-safety-fact-sheets/safe-food-handling/deep-fat-frying-and-food-safety/ct_index
15. Bacon and Food Safety. Tech. rep., United States Department of Agriculture, Food Safety and Inspection Service (2013). URL https://www.fsis.usda.gov/wps/portal/fsis/topics/food-safety-education/get-answers/food-safety-fact-sheets/meat-preparation/bacon-and-food-safety/ct_index
16. M.H. Group. Meat Temperatures Chart (2019). URL https://www.marthastewart.com/270074/meat-temperatures-chart
17. A.E. Mensch, A. Hamins, K. Markell. Time Series Data from Sensors in the Duct Above a Kitchen Cooktop During Normal Cooking and Ignition Conditions (2020). URL https://doi.org/10.18434/M32171